

AdaFlow: Imitation Learning with Variance-Adaptive Flow-Based Policies

Xixi Hu¹ Bo Liu¹ Xingchao Liu¹ Qiang Liu¹

Abstract

Diffusion-based imitation learning improves Behavioral Cloning (BC) on multi-modal decision-making, but comes at the cost of significantly slower inference due to the recursion in the diffusion process. It urges us to design efficient policy generators while keeping the ability to generate diverse actions. To address this challenge, we propose AdaFlow, an imitation learning framework based on flow-based generative modeling. AdaFlow represents the policy with state-conditioned ordinary differential equations (ODEs), which are known as probability flows. We reveal an intriguing connection between the conditional variance of their training loss and the discretization error of the ODEs. With this insight, we propose a variance-adaptive ODE solver that can adjust its step size in the inference stage, making AdaFlow an adaptive decision-maker, offering rapid inference without sacrificing diversity. Interestingly, it automatically reduces to a one-step generator when the action distribution is uni-modal. Our comprehensive empirical evaluation shows that AdaFlow achieves high performance across all dimensions, including success rate, behavioral diversity, and inference speed. The code is available at <https://github.com/hxixih/AdaFlow>

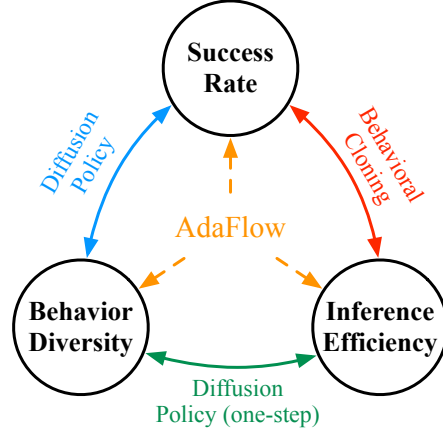


Figure 1. AdaFlow simultaneously achieves high success rate, high behavioral diversity, and high inference efficiency.

successes in training real robots (Liu et al., 2021a; Zhu et al., 2022; Brohan et al., 2022; Chi et al., 2023).

The primary approach for IL is Behavioral Cloning (BC) (Pomerleau, 1988; Ross et al., 2011; Torabi et al., 2018; Mandlekar et al., 2021), where the agent is trained with supervised learning to acquire a deterministic mapping from states to actions. Despite its simplicity, vanilla BC struggles to learn diverse behaviors in states with many possible actions (Mandlekar et al., 2021; Shafiullah et al., 2022; Chi et al., 2023; Florence et al., 2022). To improve it, various frameworks have been proposed. For instance, Implicit BC (Florence et al., 2022) learns an energy-based model for each state and searches the actions that minimize the energy with optimization algorithms. Diffuser (Janner et al., 2022; Ajay et al., 2022) and Diffusion Policy (Chi et al., 2023) adopts diffusion models (Song et al., b; Ho et al., 2020) to directly generate diverse actions.

However, the computational cost of the learned policies at the execution stage is important for an IL framework in a real-world deployment. Unfortunately, none of the previous frameworks enjoys both efficient inference and diversity. Although energy-based models and diffusion models can generate multi-modal action distributions, both of them require recursive processes to get the result. These recursive processes usually involve tens (or even hundreds) of queries before reaching their stopping criteria.

1. Introduction

Imitation Learning (IL) is a widely adopted method in robot learning (Schaal, 1999; Osa et al., 2018). In IL, an agent is given a demonstration dataset from a human expert finishing a certain task, and the goal is for it to complete the task by learning from this dataset. IL is notably effective for learning complex, non-declarative motions, yielding remarkable

¹Department of Computer Science, University of Texas at Austin, Austin, TX, United States. Correspondence to: Xixi Hu <hxixi@cs.utexas.edu>, Bo Liu <bliu@cs.utexas.edu>, Xingchao Liu <xcliu@utexas.edu>, Qiang Liu <lqiang@cs.utexas.edu>.

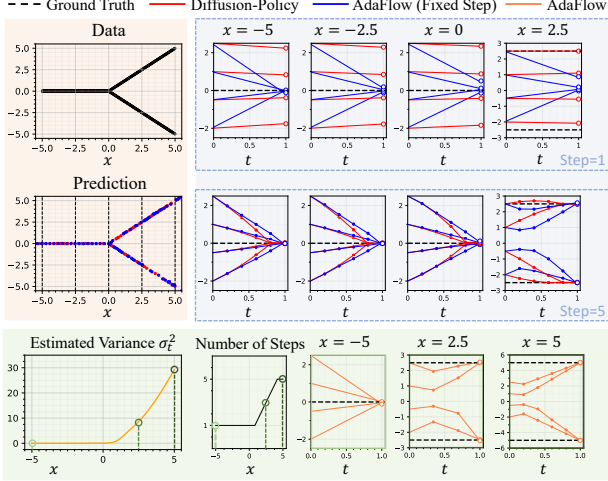


Figure 2. Illustrating the computation adaptivity of AdaFlow (orange) on simple regression task. In the upper portion of the image, we use Diffusion Policy (DDIM) and AdaFlow to predict y given x , with deterministic $y = 0$ when $x \leq 0$, and bimodal $y = \pm x$ when $x > 0$. Both DDIM and AdaFlow fit the demonstration data well. However, the simulated ODE trajectory learned by Diffusion-Policy with DDIM (red) is not straight no matter what x is. By contrast, the simulated ODE trajectory learned by AdaFlow with fixed step (blue) is a straight line when the prediction is deterministic ($x \leq 0$), which means the generation can be exactly done by one-step Euler discretization. At the bottom, we show that AdaFlow can adaptively adjust the number of simulation steps based on the x value according to the estimated variance at x .

In this paper, we propose a new IL framework, named AdaFlow, that learns a dynamic generative policy that can autonomously adjust its computation on the fly, thus cheaply outputs multi-modal action distributions to complete the task. AdaFlow is inspired by recent advancements in flow-based generative modeling (Liu et al., 2022; Lipman et al., 2022; Albergo et al., 2023; Heitz et al., 2023). We learn probability flows, which are essentially ordinary differential equations (ODEs), to represent the policies. These flows are powerful generative models that precisely capture the complicated distributions, but they still require multiple iterations to simulate the ODEs in the inference stage. To improve their efficiency, we propose an adaptive ODE solver based on the finding that the simulation error of the ODE is closely related to the variance of the training loss at different states. We train an additional small neural network to estimate the variance. During the execution of the policy, we change the step size according to the variance predicted at the current state. Equipping the flow-based policy with the proposed adaptive ODE solver, AdaFlow wisely allocates computational resources, yielding high efficiency without sacrificing the diversity provided by the flow-based generative models. Specifically, in states with deterministic action distributions, AdaFlow generates the action in *one step* – as efficient as naive BC. Empirical results on multiple bench-

marks demonstrate that AdaFlow can achieve consistently great performance across success rate, behavioral diversity, and execution efficiency.

2. Background

Imitation Learning In Imitation Learning (IL), an agent is trained to replicate an expert’s decision-making process. To formulate the problem, we assume the agent acting on a markov decision process (MDP). We denote \mathcal{S} as the state space and \mathcal{A} as the action space. A policy $\pi : \mathcal{S} \rightarrow \mathcal{A}$ maps a state to a distribution of actions. As described by Schaal (1999), the core of IL involves the agent learning from a demonstration dataset containing state-action pairs generated from an (unknown) expert policy π_E . This dataset is $D = \{(s^{(i)}, a^{(i)})\}_{i=1}^n$, where $s_t^{(i)}$ represents the state of the agent and $a^{(i)}$ is the expert’s action at state $s^{(i)}$.

The objective of an IL algorithm is to develop a parameterized policy π_θ from the dataset D . This policy, when executed, aims to generate actions that closely resemble the expert. The resemblance is quantitatively measured by minimizing a discrepancy metric between the parameterized policy π_θ and expert policy π_E . IL can be implemented in both online and offline formats. In online IL (Ho & Ermon, 2016; Fu et al., 2018), the agent interacts with the environment during the learning process. In contrast, offline IL (Torabi et al., 2018; Kostrikov et al., 2019; Mandlekar et al., 2021; Janner et al., 2022; Chi et al., 2023) restricts the agent to learning solely from the expert’s pre-recorded dataset. This work primarily focuses on offline IL for its wider application scenarios.

The most representative offline IL method is Behavioral Cloning (BC) (Pomerleau, 1988; Ross et al., 2011; Torabi et al., 2018; Mandlekar et al., 2021; Florence et al., 2022). BC is a vanilla supervised learning approach maximizing the log-likelihood objective:

$$\min_{\theta} \mathbb{E}_{(s, \mathbf{a}) \sim D} [-\log \pi_{\theta}(\mathbf{a} | s)], \quad (1)$$

where we use bold \mathbf{a} , \mathbf{s} to represent random variables. However, the vanilla BC adopts deterministic π_{θ} that can only output *one* action given a specific state, thus it does not perform well at states that allow *multi-modal* behaviors.

Recently, generative models like diffusion models (Janner et al., 2022; Wang et al., 2022; Chi et al., 2023) and energy-based models (Florence et al., 2022) have been explored to build decision-making agents for these cases. For example, Diffusion Policy (Janner et al., 2022; Chi et al., 2023) let π_{θ} be induced from a diffusion process so that the policy exhibits randomness and can sample different actions given the same state. However, these generative models are typically much more expensive than BC, in both training and deployment, calling for more efficient generative policies

that can get the best of both worlds.

Flow-based Generative Models Besides diffusion models and energy-based models, (continuous-time) flow-based generative models (Song et al., a;b; Liu et al., 2022; Lipman et al., 2022; Albergo et al., 2023; Heitz et al., 2023) also show tremendous empirical performance in generative modeling. These models employ an ordinary differential equation (ODE),

$$dz_t = v(z_t, t)dt, \quad z_0 \sim p_0, \quad (2)$$

where $v: \mathbb{R}^d \times [0, 1] \rightarrow \mathbb{R}^d$ is the velocity field parameterized by a neural network, and p_0 is a fixed initial noise distribution, such as the standard Gaussian distribution $\mathcal{N}(0, I)$. Provided a dataset drawn from an unknown distribution p_1 , the goal of learning the neural velocity v is to align the distribution of z_1 with p_1 .

Rectified flow (Liu, 2022; Liu et al., 2022) approaches this problem with a *simple supervised learning* loss function:

$$\min_v \mathbb{E}_{x_0 \sim p_0, x_1 \sim p_1} \left[\int_0^1 \|x_1 - x_0 - v(x_t, t)\|_2^2 dt \right]. \quad (3)$$

Here, $x_t = tx_1 + (1-t)x_0$ is constructed by linear interpolation between two distributions p_0 and p_1 ; the integration over t can be estimated with Monte-Carlo sampling.

Intuitively, the velocity field is optimized to follow the straight-line ODE, $dx_t = (x_1 - x_0)dt$, as much as possible. The optimal v^* satisfies $v^*(x, t) = \mathbb{E}[x_1 - x_0 \mid x_t = x]$. Integrating Eq. (2) with v^* ensures the generated marginal distribution equals the marginal distribution constructed from linear interpolation, $p_t(z_t) = p_t(x_t)$. In practice, we can parameterize v with neural networks and optimize Eq. (3) with mini-batch gradient descent. By solving the learned ODE Eq. (2) with off-the-shelf solvers, e.g., Euler method or Runge-Kutta methods, these deep flow-based models are able to generate high-quality samples in various domains (Liu et al., 2022; Wu et al., 2023; Hu et al., 2023; Guo et al., 2023). Compared with diffusion models, the generation processes of probability flows are smoother and require fewer iterative steps, making them favorable in computation-limited tasks like robotics.

3. AdaFlow for Imitation Learning

To yield an agent that enjoys both multi-modal decision-making and fast execution, we propose AdaFlow, an imitation learning framework based on flow-based generative policy. The merits of AdaFlow lie in its adaptive ability: it wisely identifies the behavioral complexity at a state before allocating computation. If the state has a deterministic choice of action, it outputs the required action rapidly; otherwise, it spends more inference time to take full advantage

of the flow-based generative policy. This handy adaptivity is made possible by leveraging a combination of elements: 1) a special property of the flow 2) a variance estimation neural network and 3) a variance-adaptive ODE solver. We formally introduce the whole framework in the sequel.

3.1. Flow-Based Generative Policy

Given the expert dataset $D = \{(s^{(i)}, a^{(i)})\}_{i=1}^n$, our goal is to learn a policy π_θ that can generate trajectories following the target distribution π_E . π_θ can be induced from a state-conditioned flow-based model,

$$dz_t = v_\theta(z_t, t \mid s)dt, \quad z_0 \sim \mathcal{N}(0, I). \quad (4)$$

Here, s is the state and the velocity field is parameterized by a neural network θ that takes the state as an additional input. To capture the expert distribution with the flow-based model, the velocity field can be trained by minimizing a state-conditioned least-squares objective,

$$L(\theta) = \mathbb{E}_{\substack{(s, \mathbf{a}) \sim D \\ \mathbf{x}_0 \sim \mathcal{N}(0, I)}} \left[\int_0^1 \|\mathbf{a} - \mathbf{x}_0 - v_\theta(\mathbf{x}_t, t \mid s)\|_2^2 dt \right], \quad (5)$$

where \mathbf{x}_t is the linear interpolation between \mathbf{x}_0 and $\mathbf{x}_1 = \mathbf{a}$:

$$\mathbf{x}_t = t\mathbf{a} + (1-t)\mathbf{x}_0. \quad (6)$$

We should differentiate z_t which is the ODE trajectory in (4) from the linear interpolation \mathbf{x}_t . They do not overlap unless all trajectories of ODE (4) are straight. See Liu et al. (2022) for more discussion.

With infinite data sampled from π_E , unlimited model capacity and perfect optimization, it is guaranteed that the policy π_θ generated from the learned flow matches the expert policy π_E (Liu et al., 2022).

3.2. The Variance-Adaptive Nature of Flow

Typically, to sample from the distribution π_θ at state s , we start with a random sample z_0 from the Gaussian distribution and simulate the ODE Eq. (4) with multi-step ODE solvers to get the action. For example, we can exploit n -step Euler discretization,

$$z_{t_{i+1}} = z_{t_i} + \frac{1}{N} v_\theta(z_{t_i}, t_i \mid s), \quad t_i = \frac{i}{N}, \quad 0 \leq i < N. \quad (7)$$

After running the solver, z_1 is the generated action. This solver requires inference with the network N times for decision-making in every state. Moreover, a large N is needed to obtain a smaller numerical error.

However, different states may have different levels of difficulty in deciding the potential actions. For instance, when traveling from a city A to another city B, there could be

multiple ways for transportation, corresponding to a multi-modal distribution of actions. After the way of transportation is chosen, the subsequent actions to take will be almost deterministic. This renders using a uniform Euler solver with the same number of inference steps N across all the states a sub-optimal solution. Rather, it is preferred that the agent can vary its decision-making process as the state of the agent changes. The challenge is how to quantitatively estimate the *complexity of a state* and employ the estimation to *adjust the inference of the flow-based policy*.

Variance as a Complexity Indicator We notice an intriguing property of the policy learned by rectified flow, which connects the complexity of a state with the training loss of the flow-based policy: if the distribution of actions is deterministic at a state s (i.e., a Dirac distribution), the trajectory of rectified flow ODE is a straight line, i.e., a *single Euler step* yields an exact estimation of \mathbf{z}_1 .

Proposition 3.1. *Let v^* be the optimum of Eq. (5). If $\text{var}_{\pi_E}(\mathbf{a} \mid s) = 0$ where $\mathbf{a} \sim \pi_E(\cdot \mid s)$, then the learned ODE conditioned on s is*

$$d\mathbf{z}_t = v^*(\mathbf{z}_t, t \mid s)dt = (\mathbf{a} - \mathbf{z}_0)dt, \quad \forall t \in [0, 1], \quad (8)$$

whose trajectories are straight lines pointing to \mathbf{z}_1 and hence can be calculated exactly with one step of Euler step:

$$\mathbf{z}_1 = \mathbf{z}_0 + v^*(\mathbf{z}_0, 0 \mid s).$$

Note that the straight trajectories of (8) satisfies $\mathbf{z}_t = t\mathbf{a} + (1-t)\mathbf{z}_0$, which makes it coincides with the linear interpolation \mathbf{x}_t . As show in Liu et al. (2022), this happens only when all the linear trajectories do not intersect on time $t \in [0, 1)$.

More generally, we can expect that the straightness of the ODE trajectories depends on how deterministic the expert policy π_E is. Moreover, the straightness can be quantified by a conditional variance metric defined as follows:

$$\begin{aligned} \sigma^2(x, t \mid s) &= \text{var}(\mathbf{a} - \mathbf{x}_0 \mid \mathbf{x}_t = x, s) \\ &= \mathbb{E} \left[\|\mathbf{a} - \mathbf{x}_0 - v^*(\mathbf{x}_t, t \mid s)\|^2 \mid \mathbf{x}_t = x, s \right]. \end{aligned} \quad (9)$$

Proposition 3.2. *Under the same condition as Proposition 3.1, we have $\sigma^2(\mathbf{z}_t, t \mid s) = 0$ following (8).*

The proof of the above propositions is in Appendix. To summarize, the variance of the state-conditioned loss function at (\mathbf{z}_t, t) can be an indicator of the multi-modality of actions. When the variance is zero, the flow-based policy can generate the expected action with only one query of the velocity field, saving a huge amount of computation. In

Algorithm 1 AdaFlow: Training

- 1: **Input:** Dataset $D = \{(s^{(i)}, a^{(i)})\}_{i=1}^N$, neural networks v_θ and σ_ϕ .
 - 2: **Stage 1: Train the flow-based policy** v_θ
 - 3: Minimize loss (5) with stochastic estimates by sampling mini-batches of $(s, \mathbf{a}) \sim D$, $\mathbf{x}_0 \sim \mathcal{N}(0, I)$ and $t \sim \text{Uni}([0, 1])$.
 - 4: **Stage 2: Train the variance estimation network** σ_ϕ
 - 5: Minimize loss (10) with stochastic estimates by sampling mini-batches of $(s, \mathbf{a}) \sim D$, $\mathbf{x}_0 \sim \mathcal{N}(0, I)$ and $t \sim \text{Uni}([0, 1])$.
-

Algorithm 2 AdaFlow: Execution

- 1: **Input:** Current state s , minimal step size ϵ_{\min} , error threshold η , pre-trained networks v_θ and σ_ϕ .
 - 2: Initialize $\mathbf{z}_0 \sim \mathcal{N}(0, I)$, $t = 0$.
 - 3: **while** $t < 1$ **do**
 - 4: Compute step size

$$\epsilon_t = \text{Clip} \left(\frac{\eta}{\sigma_\phi(\mathbf{z}_t, t \mid s)}, [\epsilon_{\min}, 1 - t] \right).$$
 - 5: Update $t \leftarrow t + \epsilon_t$, $\mathbf{z}_t \leftarrow \mathbf{z}_t + \epsilon_t v_\theta(\mathbf{z}_t, t \mid s)$.
 - 6: **end while**
 - 7: Execute action $a = \mathbf{z}_1$.
-

Section 3.3, we will show the variance can be used to bound the discretization error, thereby enabling the design of an adaptive ODE solver.

Variance Estimation Network In practice, the conditional variance $\sigma^2(x, t \mid s)$ can be empirically approximated by a neural network $\sigma_\phi^2(x, t \mid s)$ with parameter ϕ . Once the neural velocity v_θ is learned, we propose to estimate σ_ϕ by minimizing the following Gaussian negative log-likelihood loss:

$$\min_{\phi} \mathbb{E} \left[\int_0^1 \frac{\|\mathbf{a} - \mathbf{x}_0 - v_\theta(\mathbf{x}_t, t \mid s)\|^2}{2\sigma_\phi^2(\mathbf{x}_t, t \mid s)} + \log \sigma_\phi(\mathbf{x}_t, t \mid s) dt \right]. \quad (10)$$

We adopt a two-stage training strategy by first training the velocity network v_θ then the variance estimation network σ_ϕ . See Algorithm 1 for details.

3.3. Variance-Adaptive Flow-Based Policy

Because the variance indicates the straightness of the ODE trajectory, it allows us to develop an adaptive approach to

set the step size to yield better estimation with lower error during inference.

To derive our method, let us consider to advance the ODE with step size ϵ_t at \mathbf{z}_t :

$$\mathbf{z}_{t+\epsilon_t} = \mathbf{z}_t + \epsilon_t v^*(\mathbf{z}_t, t \mid s). \quad (11)$$

The problem is how to set the step size ϵ_t properly. If ϵ_t is too large, the discretized solution will significantly diverge from the continuous solution; if ϵ_t is too small, it will take excessively many steps to compute.

We propose an adaptive ODE solver based on the principle of matching the discretized marginal distribution p_t of \mathbf{z}_t from (11), and the ideal marginal distribution p_t^* when following the exact ODE (4). This is made possible with a key insight below showing that the discretization error can be bounded by the conditional variance $\sigma^2(\mathbf{z}_t, t \mid s)$.

Proposition 3.3. *Let p_t^* be the marginal distribution of the exact ODE $d\mathbf{z}_t = v^*(\mathbf{z}_t, t \mid s)dt$. Assume $\mathbf{z}_t \sim p_t = p_t^*$ and $p_{t+\epsilon_t}$ the distribution of $\mathbf{z}_{t+\epsilon_t}$ following (11). Then we have*

$$W_2(p_{t+\epsilon_t}^*, p_{t+\epsilon_t})^2 \leq \epsilon_t^2 \mathbb{E}_{\mathbf{z}_t \sim p_t} [\sigma^2(\mathbf{z}_t, t \mid s)],$$

where W_2 denotes the 2-Wasserstein distance.

We provide the proof in Appendix. Hence, given a threshold η , to ensure that an error of $W_2(p_{t+\epsilon_t}^*, p_{t+\epsilon_t})^2 \leq \eta$, we can bound the step size by $\epsilon_t \leq \eta / \sigma(\mathbf{z}_t, t \mid s)$. Because ϵ_t at time t should not be large than $1 - t$, we suggest the following rule for setting the step size ϵ_t at \mathbf{z}_t at time t :

$$\epsilon_t = \text{Clip} \left(\frac{\eta}{\sigma(\mathbf{z}_t, t \mid s)}, [\epsilon_{\min}, 1 - t] \right), \quad (12)$$

where we impose an additional lower bound ϵ_{\min} to avoid ϵ_t to be unnecessarily small. Besides, the proposed adaptive strategy guarantees to instantly arrive at the terminal point when $\sigma^2(\mathbf{z}_t, t \mid s) = 0$ as $\epsilon_t = 1 - t$. Moreover, it aligns with Section. 3.2 since for states with deterministic actions, it sets $\epsilon_0 = 1$ to generate the action in one step. We incorporate the above insights to the execution in Algorithm 2.

Global Error Analysis Proposition 3.3 provides the local error at each Euler step. In the following, we provide an analysis of the overall error for generating \mathbf{z}_1 when we simulate ODE while following the adaptive rule (12). To simplify the notation, we drop the dependency on the state s , and write $v_t^*(\cdot) = v^*(\cdot, t \mid s)$.

Assumption 3.4. *Assume $\|v_t^*\|_{Lip} \leq L$ for $t \in [0, 1]$, and the solutions of $d\mathbf{z}_t = v_t(\mathbf{z}_t)dt$ has bounded second curvature $\|\ddot{\mathbf{z}}_t\| \leq M$ for $t \in [0, 1]$.*

This is a standard assumption in numerical analysis, under which Euler’s method with a constant step size of ϵ_{\min} admits a global error of order $O(\epsilon_{\min})$.

Proposition 3.5. *Under Assumption 3.4, assume we follow Euler step (11) with step size ϵ_t in (12), starting from $\mathbf{z}_0 = \mathbf{x}_0 \sim p_0^*$. Let p_t be the distribution of \mathbf{z}_t we obtained in this way, and p_t^* that of \mathbf{x}_t in (6). Note that p_1^* is the true data distribution. Set $\eta = M_\eta \epsilon_{\min}^2 / 2$ for some $M_\eta > 0$, and $\epsilon_{\min} = 1 / N_{\max}$.*

Let N_{ada} be the number of steps we arrive at \mathbf{z}_1 following the adaptive schedule. We have

$$W_2(p_1^*, p_1) \leq C \times \frac{N_{\text{ada}}}{N_{\max}} \times \epsilon_{\min},$$

where C is a constant depending on M , M_η and L .

The idea is that the error is proportional to $\frac{N_{\text{ada}}}{N_{\max}}$, suggesting that the algorithm claims an improved error bound in the good case when it takes a smaller number of steps than the standard Euler method with constant step size ϵ_{\min} . We provide the proof in Appendix.

4. Related Work

Diffusion/Flow-based Generative Models and Adaptive Inference Diffusion models (Sohl-Dickstein et al., 2015; Ho et al., 2020; Song et al., b; Song & Ermon, 2019) succeed in various applications, e.g., image/video generation (Ho et al.; Zhang et al., 2023; Wu et al.; Saharia et al., 2022), audio generation (Kong et al.), point cloud generation (Luo & Hu, 2021a;b; Liu et al., 2023b; Wu et al., 2023), etc.. However, numerical simulation of the diffusion processes typically involve hundreds of steps, resulting in high inference cost. Post-hoc samplers have been proposed to solve this issue (Karras et al.; Liu et al., 2021b; Lu et al., 2022; Song et al., a; Bao et al., 2021) by transforming the diffusion process into marginal-preserving probability flow ODEs, yet they still use the same number of inference steps for different states. Although adaptive ODE solvers, such as adaptive step-size Runge-Kutta (Press & Teukolsky, 1992), exist, they cannot significantly reduce the number of inference steps. In comparison, the adaptive sampling strategy of AdaFlow is specifically designed based on intrinsic properties of the ODE learned rectified flow, and can achieve one-step simulation for most of the states, making it much faster for decision-making tasks in real-world applications.

Recently, new generative models (Liu et al., 2022; Liu, 2022; Lipman et al., 2022; Albergo et al., 2023; Albergo & Vanden-Eijnden, 2022; Heitz et al., 2023; Song et al., 2023; Salimans & Ho) have emerged. These models directly learn probability flow ODEs by constructing linear interpolations between two distributions, or learn to distill a pretrained diffusion model (Song et al., 2023; Salimans

& Ho) with an additional distillation training phase. Empirically, these methods exhibit more efficient inference due to their preference of straight trajectories. Among them, Rectified flow can achieve 1 step generation after reflow, a process to straighten the ODE. However, it requires synthetic data construction, which is costly.

By contrast, AdaFlow only leverages the initially learned ODE, but still keeps cheap training and inference costs that are similar to behavior cloning. We achieve this by unveiling a previously overlooked feature of these flow-based generative models: they act as one-step generators for deterministic target distributions, and their variance indicates the straightness of the probability flows for a certain state. Leveraging this feature, we design AdaFlow to automatically change the level of action modalities given on the states.

Diffusion Models for Decision Making For decision making, diffusion models obtain success as in other applications areas (Kapelyukh et al., 2023; Yang et al., 2023; Pearce et al., 2022; Chang et al., 2022). In a pioneering work, Janner et al. (2022) proposed “Diffuser”, a planning algorithm with diffusion models for offline reinforcement learning. This framework is extended to other tasks in the context of *offline reinforcement learning* (Wang et al., 2022), where the training dataset includes reward values. For example, Ajay et al. (2022) propose to model policies as conditional diffusion models. The application of DDPM (Ho et al., 2020) and DDIM (Song et al., a) on visuomotor policy learning for physical robots (Chi et al., 2023) outperforms counterparts like Behavioral Cloning. Freund et al. (2023) exploits two coupled normalizing flows to learn the distribution of expert states, and use that as a reward to train an RL agent for imitation learning. AdaFlow admits a much simpler training and inference pipeline compared with it. Despite the success of adopting generative diffusion models as decision makers in previous works, they also bring redundant computation, limiting their application in real-time, low-latency decision-making scenarios for autonomous robots. AdaFlow propose to leverage rectified flow instead of diffusion models, facilitating adaptive decision making for different states while significantly reducing computational requirements. In this work, similar to Diffusion Policy (Chi et al., 2023), we focus on offline imitation learning. While AdaFlow could theoretically be adapted for offline reinforcement learning, we leave it for future works.

5. Experiments

We conducted experiments to comprehensively evaluate AdaFlow against BC and diffusion policy along three dimensions: task performance, behavior diversity, and training/inference efficiency. In what follows, we first present the metrics for each dimension and then validate the perfor-

mance of each IL method on four sets of tasks: **1)** a simple 1D toy example to demonstrate AdaFlow computational adaptivity; **2)** a 2D navigation problem that offers clear visualization of different methods’ behavior; and the more practical robot manipulation tasks on **3)** RoboMimic (Ajay et al., 2022) and **4)** LIBERO (Liu et al., 2021a).

5.1. Baselines

We mainly compare AdaFlow against 1) behavioral cloning (BC) and 2) Diffusion Policy (Chi et al., 2023) (Diff- π). For Diff- π , we consider both the DDPM and DDIM variants, and additionally with a varying number of NFE in DDIM.

5.2. Evaluation Metrics

We consider the following four evaluation metrics.

Success Rate (SR) To assess the precision of π_θ , we randomly sample the start states s_0 , then get the rollout of π_θ starting from s_0 , and finally record the expected success rate over a fixed number of episodes.

Diversity Score (DS) We measure how diverse the learned behavior is with a novel *diversity score*. In short, we first define a divergence between two sets of states. Then we measure how much portion of the demonstration set can be covered by the learned policy, according to the defined divergence. Specifically, for two sets of states τ_1 and τ_2 , define $d(\tau_1, \tau_2) = \frac{1}{|\tau_1|} \sum_{s_1 \sim \tau_1} \min_{s_2 \in \tau_2} \|s_1 - s_2\|^2$, i.e., the average distance of each point in τ_1 to τ_2 . Then define

$$\lambda_{\text{expert}} = \max_k d(D_k^i, \{D_j\}_{j \neq k}). \quad (13)$$

Here, D_k^i is the i -th observation in the k -th demonstration, $\{D_j\}_{j \neq k}$ denotes all other demonstration observations excluding the k -th demonstration trajectory. λ_{expert} roughly measures the maximal distance of each demonstration trajectory to the rest of the demonstration set. Then, we compute the diversity score (DS) as:

$$\text{DS} = \frac{1}{K} \sum_{k=1}^K \mathbb{1} [d(D_k^i, \rho(\pi_\theta)) \leq \lambda_{\text{expert}}], \quad (14)$$

where $\rho(\pi_\theta)$ denotes the rollouts trajectories of π_θ , and $\mathbb{1}(\cdot)$ is the indicator function. In short, DS measures how much portion of the demonstration set has a closer divergence to $\rho(\pi_\theta)$ than to the rest of the demonstration. During diversity evaluation, we fix the agent’s start state, and $\rho(\pi_\theta)$ is set to the states generated in 50 rollouts of π_θ .

Training and Execution Efficiency The execution efficiency is evaluated by the number of function evaluations (NFE). The training efficiency is visualized as the area under the curve of the success rate versus epochs. Details are provided in Section 5.6.

5.3. Regression

We start with a 1D regression task designed to demonstrate the adaptivity nature of AdaFlow. The goal is to learn a mapping from x to y where

$$y = \begin{cases} 0 & \text{for } x \leq 0 \\ \pm x & \text{for } x > 0. \end{cases} \quad (15)$$

Note that $y \mid x$ is deterministic when $x \leq 0$ and stochastic otherwise. The training and testing data are uniformly sampled from the ground-truth function with $x \in [-5, 5]$. Details about the setup and the hyperparameters are provided in Appendix.

Results Figure 2 (top-right) shows the generation trajectories of Diff- π and AdaFlow with fixed step. Notably, when $x \leq 0$, AdaFlow generates *straight* trajectories (step = 1 or 5) and is therefore able to predict y with a single step, aligning our analysis in Proposition 3.1 and 3.2. In contrast, Diff- π fails to predict y accurately with a single step, while generating curved trajectories when step = 5. The bottom of Figure 2 shows the estimated variance by AdaFlow across $x \in [-5, 5]$, which accurately aligns with the expected variance. In addition, as x increases, AdaFlow adaptively increases the required number of simulation steps.

5.4. Navigating a 2D Maze

We create two sets of maze navigation tasks to validate AdaFlow’s performance of modeling multi-modal behavior. In particular, we create two *single-task* environments where the agent starts and ends at a fixed point and two *multi-task* environments where the agent can start and end at different points. All four environments are simulated in D4RL Maze2D (Fu et al., 2020) using MuJoCo. The environments and demonstrations are visualized in Figure 6. We measure both SR and DS for the single-task mazes and only SR for the multi-task mazes, as it is difficult to accurately define DS in the multi-task setting.

Results We compare AdaFlow against baseline methods in Table 1. From the table, we see that AdaFlow with an average NFE of 1.56 NFE can achieve highly diverse behavior in terms of DS and a near-perfect success rate in the meantime. Moreover, the DS is not dropping and the SR remains strong when the average NFE drops to 1.12. By contrast, Diff- π only demonstrates diverse behavior when NFE is larger than 5 and falls behind in SR even with 20 NFE compared to AdaFlow. BC, on the other hand, has high SR while performing relatively poorly in terms of DS. We additionally visualize the rollout trajectories from each learned policy in Figure 3 as a qualitative comparison of the learned behavior across different methods.

Table 1. Performance on maze navigation tasks. The table shows the success rate (SR) for each model across different maze complexities. Additionally, for single-task mazes (e.g., Maze 1 and Maze 2), we evaluate the diversity score (DS) to reflect the model’s capacity to learn diverse behavior. The highest success rate and diversity score for each task are highlighted in **bold**.

Method	NFE↓	Maze 1	Maze 2	Maze 3	Maze 4
		SR↑ / DS↑	SR↑ / DS↑	SR↑	SR↑
Diff- π (DDPM)	20	0.62 / 0.99	0.98 / 0.98	0.84	0.82
Diff- π (DDIM)	5	0.58 / 0.99	1.00 / 0.96	0.84	0.76
Diff- π (DDIM)	1	0.00 / 0.68	0.32 / 0.62	0.16	0.08
BC	1	1.00 / 0.43	1.00 / 0.24	0.92	0.76
AdaFlow ($\eta = 1.5$)	1.56	0.98 / 0.92	1.00 / 0.86	0.96	0.86
AdaFlow ($\eta = 2.5$)	1.12	1.00 / 0.91	1.00 / 0.85	0.94	0.78

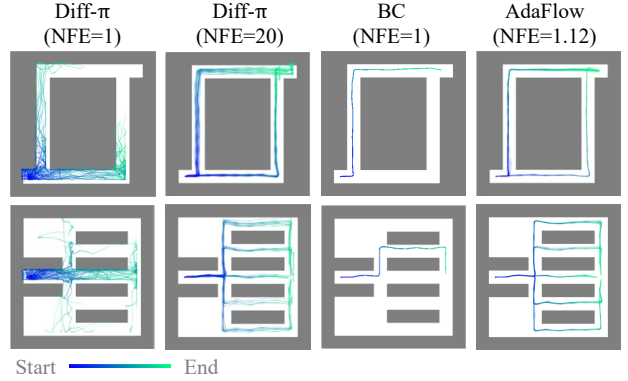


Figure 3. **Generated trajectories.** We visualize the trajectories generated by various policies, with the agent’s starting point fixed.

5.5. Robot Manipulation Tasks

Environments and Tasks To further validate how AdaFlow performs on practical robotics tasks, we compare AdaFlow against baselines on a Push-T task (Chi et al., 2023), the RoboMimic (Mandlekar et al., 2021) benchmark (Lift, Can, Square, Transport, ToolHang) and the LIBERO (Liu et al., 2023a) benchmark. For the Push-T task and the tasks in RoboMimic, we follow the exact experimental setup described in Diffusion Policy (Chi et al., 2023). Following the Diffusion Policy, we add three additional baseline methods: 1) LSTM-GMM, BC with the LSTM model and a Gaussian mixture head, 2) IBC, the implicit behavioral cloning (Florence et al., 2022), an energy-based model for generative decision-making, and 3) BET (Shafiullah et al., 2022). For the LIBERO tasks, we pick a subset of six Kitchen tasks and follow the setup described in the original paper (Check Figure 7 for the description of the six tasks), but adapting the learning algorithm from BC to AdaFlow and Diff- π .

Results The results of the Push-T task and the RoboMimic benchmark are summarized in Table 3. We only show the results here for the Square, Transport, ToolHang, and Push-T tasks, as on the Lift and Can task we observe no notice-

Table 2. Performance Evaluation on the LIBERO Benchmark. The highest success rate for each task are highlighted in **bold**.

Method	NFE↓	Task 1	Task 2	Task 3	Task 4	Task 5	Task 6	Average
		SR↑ / DS↑	SR↑ / DS↑	SR↑ / DS↑	SR↑ / DS↑	SR↑ / DS↑	SR↑ / DS↑	SR↑ / DS↑
BC	1	0.88 / 0.60	0.80 / 0.68	0.96 / 0.69	0.78 / 0.59	0.92 / 0.88	0.82 / 0.61	0.86 / 0.67
Diff- π	20	0.94 / 0.94	0.84 / 0.83	0.98 / 0.78	0.78 / 0.79	0.82 / 0.93	0.92 / 0.87	0.88 / 0.85
Diff- π	1	0.00 / 1.00	0.00 / 1.00	0.00 / 1.00	0.00 / 1.00	0.00 / 1.00	0.00 / 1.00	0.00 / 1.00
Diff- π	2	0.00 / 1.00	0.58 / 0.96	0.36 / 0.97	0.66 / 0.97	0.36 / 0.94	0.32 / 0.86	0.38 / 0.95
AdaFlow	1.27	0.98 / 0.95	0.80 / 0.80	0.98 / 0.76	0.82 / 0.85	0.90 / 0.94	0.96 / 0.87	0.91 / 0.86

 Table 3. Success rate (SR↑) on the RoboMimic Benchmark. The highest success rate for each task are highlighted in **bold**. For tasks marked with *, we train all the models (BC, Diff- π , AdaFlow) for 500 epochs due to prohibitive training cost.

Method	NFE↓	Square ph / mh	Transport* ph / mh	ToolHang* ph	Push-T ph
LSTM-GMM	1	0.95 / 0.86	0.76 / 0.62	0.67	0.69
IBC	1	0.00 / 0.00	0.00 / 0.00	0.00	0.75
BET	1	0.76 / 0.68	0.38 / 0.21	0.58	-
<i>Same network architecture</i>					
BC	1	0.92 / 0.96	0.90 / 0.80	0.78	0.98
Diff- π	100	1.00 / 0.97	0.90 / 0.72	0.90	0.91
Diff- π	1	0.00 / 0.00	0.00 / 0.00	0.00	0.04
Diff- π	2	0.56 / 0.12	0.84 / 0.68	0.68	0.34
AdaFlow	1.17	0.98 / 0.96	0.92 / 0.80	0.88	0.96

able differences among different methods. For full results on RoboMimic and more implementation details, see Appendix. From the table, we observe that AdaFlow consistently achieves comparable or higher success rates across different challenging manipulation tasks, compared against all baselines, with only an average NFE of 1.17. Note that Diff- π , while showing high success rates using NFE = 100, falls behind when NFE = 1.

Results for the six LIBERO tasks are presented in Table 2. Aligning with findings from our previous experiments, AdaFlow once again outperforms BC and Diff- π in terms of SR, and maintains a high DS across all environments, with an average NFE of 1.27. We additionally visualize the variance predicted by AdaFlow in Figure 4. It can be seen that the model identifies the high variance when the robot’s end effector is close to the object or target area, matching the expected variance from the demonstration set.

5.6. Ablation Study

We present additional experiments to examine AdaFlow on all four dimensions: SR, DS, training, and inference efficiency. We pick Maze 2 from the 2D navigation task for comparison. The results are provided in Figure 5.

Results Figure 5 (top-left) compares the DS and SR of 1-step models. AdaFlow is the only method that achieves high DS and SR simultaneously. Figure 5 (top-right) evaluates the training efficiency by showing SR over epochs. We see

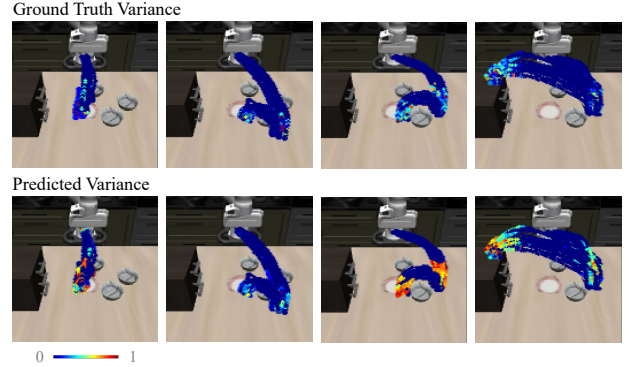


Figure 4. **Predicted variance.** We visualize the variance predicted by AdaFlow. The variance is computed on states from the expert’s demonstration and averaged over all simulation steps (e.g., t from 0 to 1). Then we normalize the variance to $[0, 1]$ by the largest variance found at all states.

that AdaFlow achieves better area-under-curve than Diff- π , indicating that it learns faster than Diff- π . Expectedly, BC achieves the best learning efficiency due to its simplicity. Figure 5 (bottom-left and bottom-right) explores how DS and SR change over the number of function evaluations (NFE). We observe that AdaFlow achieves both high DS and SR with very low NFE, while Diff- π in general requires more than 3 NFEs to achieve a good performance. BC achieves high SR with a single NFE, but demonstrates very poor behavioral diversity in terms of DS. Additionally, for AdaFlow, as the NFEs are computed under different values of η , both plots demonstrate that AdaFlow is robust to the value of η .

6. Conclusion

In conclusion, we present AdaFlow, a novel imitation learning algorithm adept at efficiently generating diverse and adaptive policies, addressing the trade-off between computational efficiency and behavioral diversity inherent in current models. Through extensive experimentation across various settings, AdaFlow demonstrated superior performance across multiple dimensions including success rate, behavioral diversity, and training/execution efficiency. This work lays a robust foundation for future research on adaptive imitation learning methods in real-world scenarios.

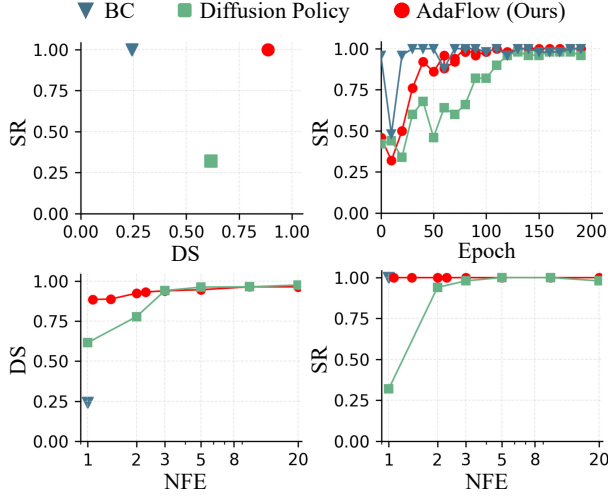


Figure 5. Ablation studies on AdaFlow.

7. Broader Impact

This paper propose a new framework for imitation learning, which aims at training fast agents that can make diverse decisions. While we acknowledge that our work could have a multitude of potential societal consequences, we do not believe there are any specific ones that need to be highlighted in this context.

References

- Ajay, A., Du, Y., Gupta, A., Tenenbaum, J. B., Jaakkola, T. S., and Agrawal, P. Is conditional generative modeling all you need for decision making? In *The Eleventh International Conference on Learning Representations*, 2022.
- Albergo, M. S. and Vanden-Eijnden, E. Building normalizing flows with stochastic interpolants. In *The Eleventh International Conference on Learning Representations*, 2022.
- Albergo, M. S., Boffi, N. M., and Vanden-Eijnden, E. Stochastic interpolants: A unifying framework for flows and diffusions. *arXiv preprint arXiv:2303.08797*, 2023.
- Bao, F., Li, C., Zhu, J., and Zhang, B. Analytic-dpm: an analytic estimate of the optimal reverse variance in diffusion probabilistic models. In *International Conference on Learning Representations*, 2021.
- Brohan, A., Brown, N., Carbajal, J., Chebotar, Y., Dabis, J., Finn, C., Gopalakrishnan, K., Hausman, K., Herzog, A., Hsu, J., et al. Rt-1: Robotics transformer for real-world control at scale. *arXiv preprint arXiv:2212.06817*, 2022.
- Chang, W.-D., Higuera, J. C. G., Fujimoto, S., Meger, D., and Dudek, G. Il-flow: Imitation learning from observation using normalizing flows. *arXiv preprint arXiv:2205.09251*, 2022.
- Chi, C., Feng, S., Du, Y., Xu, Z., Cousineau, E., Burchfiel, B., and Song, S. Diffusion policy: Visuomotor policy learning via action diffusion. *arXiv preprint arXiv:2303.04137*, 2023.
- Florence, P., Lynch, C., Zeng, A., Ramirez, O. A., Wahid, A., Downs, L., Wong, A., Lee, J., Mordatch, I., and Tompson, J. Implicit behavioral cloning. In *Conference on Robot Learning*, pp. 158–168. PMLR, 2022.
- Freund, G. J., Sarafian, E., and Kraus, S. A coupled flow approach to imitation learning. In *International Conference on Machine Learning*, pp. 10357–10372. PMLR, 2023.
- Fu, J., Luo, K., and Levine, S. Learning robust rewards with adversarial inverse reinforcement learning. In *International Conference on Learning Representations*, 2018.
- Fu, J., Kumar, A., Nachum, O., Tucker, G., and Levine, S. D4rl: Datasets for deep data-driven reinforcement learning. *arXiv preprint arXiv:2004.07219*, 2020.
- Guo, Y., Du, C., Ma, Z., Chen, X., and Yu, K. Voiceflow: Efficient text-to-speech with rectified flow matching. *arXiv preprint arXiv:2309.05027*, 2023.
- Heitz, E., Belcour, L., and Chambon, T. Iterative α - (de)blending: A minimalist deterministic diffusion model. In *ACM SIGGRAPH 2023 Conference Proceedings*, SIGGRAPH '23, New York, NY, USA, 2023. Association for Computing Machinery. ISBN 9798400701597. doi: 10.1145/3588432.3591540. URL <https://doi.org/10.1145/3588432.3591540>.
- Ho, J. and Ermon, S. Generative adversarial imitation learning. *Advances in neural information processing systems*, 29, 2016.
- Ho, J., Salimans, T., Gritsenko, A. A., Chan, W., Norouzi, M., and Fleet, D. J. Video diffusion models. In *Advances in Neural Information Processing Systems*.
- Ho, J., Jain, A., and Abbeel, P. Denoising diffusion probabilistic models. *Advances in neural information processing systems*, 33:6840–6851, 2020.
- Hu, V. T., Yin, W., Ma, P., Chen, Y., Fernando, B., Asano, Y. M., Gavves, E., Mettes, P., Ommer, B., and Snoek, C. G. Motion flow matching for human motion synthesis and editing. *arXiv preprint arXiv:2312.08895*, 2023.
- Janner, M., Du, Y., Tenenbaum, J., and Levine, S. Planning with diffusion for flexible behavior synthesis. In *International Conference on Machine Learning*, pp. 9902–9915. PMLR, 2022.

- Kapelyukh, I., Vosylius, V., and Johns, E. Dall-e-bot: Introducing web-scale diffusion models to robotics. *IEEE Robotics and Automation Letters*, 2023.
- Karras, T., Aittala, M., Aila, T., and Laine, S. Elucidating the design space of diffusion-based generative models. In *Advances in Neural Information Processing Systems*.
- Kong, Z., Ping, W., Huang, J., Zhao, K., and Catanzaro, B. Diffwave: A versatile diffusion model for audio synthesis. In *International Conference on Learning Representations*.
- Kostrikov, I., Nachum, O., and Tompson, J. Imitation learning via off-policy distribution matching. In *International Conference on Learning Representations*, 2019.
- Lipman, Y., Chen, R. T., Ben-Hamu, H., Nickel, M., and Le, M. Flow matching for generative modeling. In *The Eleventh International Conference on Learning Representations*, 2022.
- Liu, B., Xiao, X., and Stone, P. A lifelong learning approach to mobile robot navigation. *IEEE Robotics and Automation Letters*, 6(2):1090–1096, 2021a.
- Liu, B., Zhu, Y., Gao, C., Feng, Y., Liu, Q., Zhu, Y., and Stone, P. Libero: Benchmarking knowledge transfer for lifelong robot learning. *arXiv preprint arXiv:2306.03310*, 2023a.
- Liu, L., Ren, Y., Lin, Z., and Zhao, Z. Pseudo numerical methods for diffusion models on manifolds. In *International Conference on Learning Representations*, 2021b.
- Liu, Q. Rectified flow: A marginal preserving approach to optimal transport. *arXiv preprint arXiv:2209.14577*, 2022.
- Liu, X., Gong, C., and Liu, Q. Flow straight and fast: Learning to generate and transfer data with rectified flow. In *The Eleventh International Conference on Learning Representations*, 2022.
- Liu, X., Wu, L., Ye, M., et al. Learning diffusion bridges on constrained domains. In *The Eleventh International Conference on Learning Representations*, 2023b.
- Lu, C., Zhou, Y., Bao, F., Chen, J., Li, C., and Zhu, J. Dpm-solver: A fast ode solver for diffusion probabilistic model sampling in around 10 steps. In *Advances in Neural Information Processing Systems*.
- Lu, C., Zhou, Y., Bao, F., Chen, J., Li, C., and Zhu, J. Dpm-solver++: Fast solver for guided sampling of diffusion probabilistic models. *arXiv preprint arXiv:2211.01095*, 2022.
- Luo, S. and Hu, W. Diffusion probabilistic models for 3d point cloud generation. In *Proceedings of the IEEE/CVF Conference on Computer Vision and Pattern Recognition*, pp. 2837–2845, 2021a.
- Luo, S. and Hu, W. Score-based point cloud denoising. In *Proceedings of the IEEE/CVF International Conference on Computer Vision*, pp. 4583–4592, 2021b.
- Mandlekar, A., Xu, D., Wong, J., Nasiriany, S., Wang, C., Kulkarni, R., Fei-Fei, L., Savarese, S., Zhu, Y., and Martín-Martín, R. What matters in learning from offline human demonstrations for robot manipulation. *arXiv preprint arXiv:2108.03298*, 2021.
- Osa, T., Pajarinen, J., Neumann, G., Bagnell, J. A., Abbeel, P., Peters, J., et al. An algorithmic perspective on imitation learning. *Foundations and Trends® in Robotics*, 7(1-2):1–179, 2018.
- Pearce, T., Rashid, T., Kanervisto, A., Bignell, D., Sun, M., Georgescu, R., Macua, S. V., Tan, S. Z., Momennejad, I., Hofmann, K., et al. Imitating human behaviour with diffusion models. In *Deep Reinforcement Learning Workshop NeurIPS 2022*, 2022.
- Pomerleau, D. A. Alvin: An autonomous land vehicle in a neural network. *Advances in neural information processing systems*, 1, 1988.
- Press, W. H. and Teukolsky, S. A. Adaptive stepsize runge-kutta integration. *Computers in Physics*, 6(2):188–191, 1992.
- Ross, S., Gordon, G., and Bagnell, D. A reduction of imitation learning and structured prediction to no-regret online learning. In *Proceedings of the fourteenth international conference on artificial intelligence and statistics*, pp. 627–635. JMLR Workshop and Conference Proceedings, 2011.
- Saharia, C., Chan, W., Saxena, S., Li, L., Whang, J., Denton, E. L., Ghasemipour, K., Gontijo Lopes, R., Karagol Ayan, B., Salimans, T., et al. Photorealistic text-to-image diffusion models with deep language understanding. *Advances in Neural Information Processing Systems*, 35: 36479–36494, 2022.
- Salimans, T. and Ho, J. Progressive distillation for fast sampling of diffusion models. In *International Conference on Learning Representations*.
- Schaal, S. Is imitation learning the route to humanoid robots? *Trends in cognitive sciences*, 3(6):233–242, 1999.
- Shafiuallah, N. M., Cui, Z., Altanzaya, A. A., and Pinto, L. Behavior transformers: Cloning k modes with one stone. *Advances in neural information processing systems*, 35: 22955–22968, 2022.

- Sohl-Dickstein, J., Weiss, E., Maheswaranathan, N., and Ganguli, S. Deep unsupervised learning using nonequilibrium thermodynamics. In *International Conference on Machine Learning*, pp. 2256–2265. PMLR, 2015.
- Song, J., Meng, C., and Ermon, S. Denoising diffusion implicit models. In *International Conference on Learning Representations*, a.
- Song, Y. and Ermon, S. Generative modeling by estimating gradients of the data distribution. *Advances in neural information processing systems*, 32, 2019.
- Song, Y., Sohl-Dickstein, J., Kingma, D. P., Kumar, A., Ermon, S., and Poole, B. Score-based generative modeling through stochastic differential equations. In *International Conference on Learning Representations*, b.
- Song, Y., Dhariwal, P., Chen, M., and Sutskever, I. Consistency models. 2023.
- Torabi, F., Warnell, G., and Stone, P. Behavioral cloning from observation. In *Proceedings of the Twenty-Seventh International Joint Conference on Artificial Intelligence*. International Joint Conferences on Artificial Intelligence Organization, 2018.
- Wang, Z., Zheng, H., He, P., Chen, W., and Zhou, M. Diffusion-gan: Training gans with diffusion. In *The Eleventh International Conference on Learning Representations*, 2022.
- Wu, L., Gong, C., Liu, X., Ye, M., et al. Diffusion-based molecule generation with informative prior bridges. In *Advances in Neural Information Processing Systems*.
- Wu, L., Wang, D., Gong, C., Liu, X., Xiong, Y., Ranjan, R., Krishnamoorthi, R., Chandra, V., and Liu, Q. Fast point cloud generation with straight flows. In *Proceedings of the IEEE/CVF Conference on Computer Vision and Pattern Recognition*, pp. 9445–9454, 2023.
- Yang, S., Nachum, O., Du, Y., Wei, J., Abbeel, P., and Schuurmans, D. Foundation models for decision making: Problems, methods, and opportunities. *arXiv preprint arXiv:2303.04129*, 2023.
- Zhang, S., Yang, X., Feng, Y., Qin, C., Chen, C.-C., Yu, N., Chen, Z., Wang, H., Savarese, S., Ermon, S., Xiong, C., and Xu, R. Hive: Harnessing human feedback for instructional visual editing. *arXiv preprint arXiv:2303.09618*, 2023.
- Zhu, Y., Joshi, A., Stone, P., and Zhu, Y. Viola: Imitation learning for vision-based manipulation with object proposal priors. *6th Annual Conference on Robot Learning (CoRL)*, 2022.

A. Appendix

A.1. Proof of Proposition 3.1 and Proposition 3.2.

Proof. $\text{var}_{\pi_E}(\mathbf{a}|s) = 0$ means that the action $\mathbf{a} = a$ equals a deterministic value a given s . With $\mathbf{x}_t = t\mathbf{a} + (1-t)\mathbf{x}_0$, note that

$$\mathbf{a} - \mathbf{x}_0 = \frac{1}{1-t}(\mathbf{a} - \mathbf{x}_t).$$

Therefore, $\mathbf{a} - \mathbf{x}_0$ is deterministically decided by \mathbf{x}_t and s . This yields

$$v^*(x, t | s) = \mathbb{E}[a - \mathbf{x}_0 | \mathbf{x}_t = x] = \frac{1}{1-t}(a - x).$$

Therefore, we have

$$d\mathbf{z}_t = v^*(\mathbf{z}_t, t | s) = \frac{1}{1-t}(a - \mathbf{z}_t)dt.$$

Solving ODE this yields

$$\mathbf{z}_t = t\mathbf{a} + (1-t)\mathbf{z}_0 = (1-t)v^*(\mathbf{z}_0, 0 | s).$$

Differentiating it also yields

$$\mathbf{z}_t = (a - \mathbf{z}_0)dt.$$

We also have $\sigma^2(x, t | s)$ again because $a - \mathbf{x}_0$ is deterministic given \mathbf{x}_t and s :

$$\sigma^2(x, t | s) = \text{var}(\mathbf{a} - \mathbf{x}_0 | \mathbf{x}_t = x, s) = 0.$$

□

A.2. Proof of Proposition 3.3

Proof of Proposition 3.3. Following the property of rectified flow, the distribution of $\mathbf{x}_1 = t\mathbf{a} + (1-t)\mathbf{x}_0$ coincides with p_t for all $t \in [0, 1]$. Hence, we can assume that $\mathbf{z}_t = \mathbf{x}_t \sim p_t^*$. In this case, we have $\mathbf{z}_{t+\epsilon_t} = \mathbf{x}_t + \epsilon_t v^*(\mathbf{z}_t, t | s)$ and $\mathbf{x}_{t+\epsilon_t} = \mathbf{x}_t + \epsilon_t(\mathbf{a} - \mathbf{x}_0)$. We have

$$\begin{aligned} & W_2(p_{t+\epsilon_t}^*, p_{t+\epsilon_t})^2 \\ & \leq \mathbb{E} \left[\|\mathbf{z}_{t+\epsilon_t} - \mathbf{x}_{t+\epsilon_t}\|_2^2 \right] \\ & = \mathbb{E} \left[\mathbb{E} \left[\|\mathbf{z}_{t+\epsilon_t} - \mathbf{x}_{t+\epsilon_t}\|_2^2 | \mathbf{x}_t \right] \right] \\ & = \mathbb{E} \left[\mathbb{E} \left[\|\epsilon_t v^*(\mathbf{z}_t, t | s) - \epsilon_t(\mathbf{a} - \mathbf{x}_0)\|_2^2 | \mathbf{x}_t \right] \right] \\ & = \epsilon_t^2 \mathbb{E}_{\mathbf{z}_t \sim p_t} [\sigma^2(\mathbf{z}_t, t | s)]. \end{aligned}$$

□

A.3. Proof of Proposition 3.5

Proof. Assume the adaptive algorithm visits the time grid of $0 = t_0, t_1, \dots, t_N = 1$.

Define $\mathbf{z}_t^{t_i}$ be the result when we implement the adaptive discretization algorithm upto t_i and then switch to follow the exact ODE afterward, that is, we have $d\mathbf{z}_t^{t_i} = v_t(\mathbf{z}_t^{t_i})dt$ for $t \geq t_i$. In this way, we have $\mathbf{z}_t^1 = \mathbf{z}_t$, and $\mathbf{z}_t^0 = \mathbf{z}_t^*$, where \mathbf{z}_t^* is the trajectory of the exact ODE $d\mathbf{z}_t^* = v_t^*(\mathbf{z}_t^*)dt$.

From Lemma A.1, we have

$$\left\| \mathbf{z}_1^{t_{i-1}} - \mathbf{z}_1^{t_i} \right\| \leq \exp(L(1-t_i)) \left\| \mathbf{z}_{t_i}^{t_i} - \mathbf{z}_{t_i}^{t_{i-1}} \right\|.$$

Let $p_t^{t_i}$ be the distribution of $z_t^{t_i}$. Then we have $p_t^1 = p_t$ and $p_t^0 = p_t^*$. Then

$$\begin{aligned} W_2(p_1^{t_{i-1}}, p_1^{t_i}) &\leq \mathbb{E} \left[\left\| z_1^{t_{i-1}} - z_1^{t_i} \right\|^2 \right]^{1/2} \\ &= \exp(L(1 - t_i)) \mathbb{E} \left[\left\| z_{t_i}^{t_{i-1}} - z_{t_i}^{t_i} \right\|^2 \right]^{1/2} \\ &= \exp(L(1 - t_i)) \max(\eta, \epsilon_{\min}^2 M/2) \\ &= C \epsilon_{\min}^2 \exp(-Lt_i), \end{aligned}$$

where $C = \frac{1}{2} \max(M, M_\eta) \exp(L(1 - t_i))$. Here we use the bound in the proof of Proposition 3.1 and Lemma A.1. Hence,

$$\begin{aligned} W_2(p_1^*, p_1) &= \sum_{i=1}^{N_{\text{ada}}} W_2(p_1^{t_{i-1}}, p_1^{t_i}) \\ &\leq \sum_{i=1}^{N_{\text{ada}}} C \epsilon_{\min}^2 \exp(-Lt_i) \\ &\leq C \times \frac{N_{\text{ada}}}{N_{\text{max}}} \times \epsilon_{\min}, \end{aligned}$$

where $C = \exp(L) \max(M, M_\eta)$. □

Lemma A.1. *Let $\|v_t\|_{Lip} \leq L$ for $t \in [0, 1]$. Assume x_t and y_t solve $dx_t = v_t(x_t)dt$ and $dy_t = v_t(y_t)dt$ starting from x_0, y_0 , respectively. We have*

$$\|x_t - y_t\| \leq \exp(Lt) \|x_0 - y_0\|, \quad \forall t \in [0, 1]. \quad (16)$$

Proof.

$$\begin{aligned} \frac{d}{dt} \|x_t - y_t\|^2 &= 2(x_t - y_t)^\top (v_t(x_t) - v_t(y_t)) \\ &\leq 2L \|x_t - y_t\|^2, \end{aligned}$$

where we used $\|v_t(x_t) - v_t(y_t)\| \leq L \|x_t - y_t\|$. Using Gronwall's inequality yields the result. □

Lemma A.2. *Under Assumption 3.4, we have*

$$\|x_{t+\epsilon} - (x_t + \epsilon v_t(x_t))\| \leq \frac{\epsilon^2 M}{2},$$

for $0 \leq t \leq \epsilon + t \leq 1$.

Proof. Direct application of Taylor approximation. □

A.4. Visualization of Tasks

In this section, we provide a visualization of the 2D Maze and LIBERO tasks in Figure 6 and Figure 7.

A.5. Planner for Maze2D task

We generate the demonstration data in Maze toy using planner similar to (Fu et al., 2020). The planner devises a path in a maze environment by calculating waypoints between the start and target points. It begins by transforming the given continuous-state space into a discretized grid representation. Employing Q-learning, it evaluates the optimal actions and subsequently computes the waypoints by performing a rollout in the grid, introducing random perturbations to the waypoints for diversity. The controller connects these waypoints in an ordered manner to form a feasible path. In runtime, it dynamically adjusts the control action based on the proximity to the next waypoint and switches waypoints when close enough, ensuring the trajectory remains adaptive and efficient.

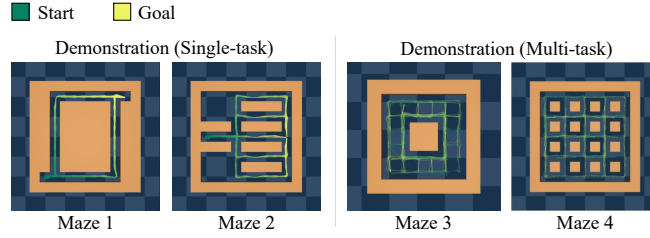
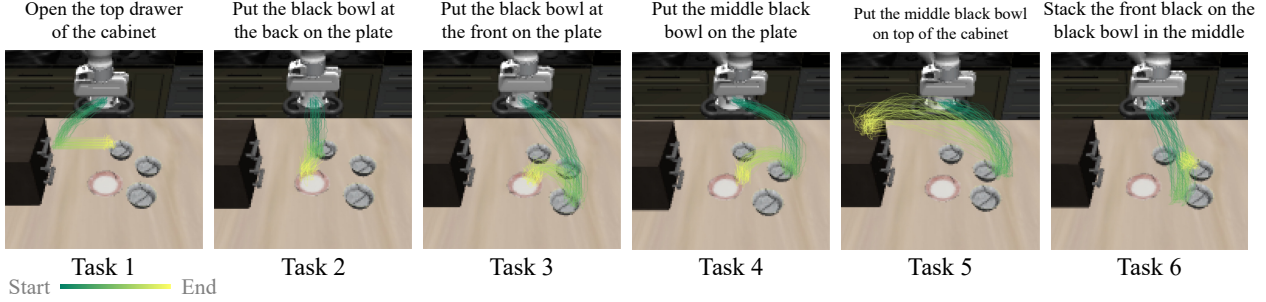


Figure 6. Trajectories of 100 demonstrations for each maze.

Figure 7. **LIBERO tasks.** We visualize the demonstrated trajectories of the robot’s end effector.

A.6. Comparative Analysis of Separate and Joint Training

In this section, we provide a comparison between the two training strategies employed in our proposed solution: separate training and joint training. Our primary objective is to investigate whether there is a substantial difference in performance and efficiency between these two training approaches.

Experiment Setup. To conduct this comparative analysis, we designed experiments using our proposed framework with both training strategies. Specifically, we consider two approaches: separate and joint training. In **Separate Training** setting, we train the variance prediction network and the policy function separately, as described in our main paper. In **Joint Training** setting, we train both the variance prediction network and the policy function simultaneously in an end-to-end manner. The goal is to assess the impact of these training strategies on the overall performance.

Results and Discussion. As shown in Table 4, the performance were consistent between the two training approaches, indicating the effectiveness of our two-stage framework in balancing policy accuracy and uncertainty estimation. Separate training exhibited faster computational speed, making it the preferred choice once the policy function was robustly trained. Joint training required more computational resources and time.

Table 4. Performance comparison of separate training and joint training of AdaFlow in Maze tasks. The table presents key performance metrics, including Success Rate (SR), Diversity Score (DS), Number of Function Evaluations (NFE), and Learning Efficiency Index (LEI), across various maze complexities. Results are shown for each model in different maze scenarios, as well as the average performance.

	Maze 1		Maze 2		Maze 3	Maze 4
	SR	DS	SR	DS	SR	SR
AdaFlow (Separate)	0.98	0.92	1.00	0.86	0.96	0.86
AdaFlow (Joint)	1.00	0.90	1.00	0.87	0.96	0.88

A.7. Visualization of Exact Variance.

In the main paper, we showed the variance predictions made by RF-POLICY across different states within a robot’s state space. Here, we explain how we compute the *exact* variance for different states, to provide a ground truth of variance for reference. To achieve this, we first train a 1-Rectified Flow model for the task, then we can compute the exact variance by sampling according to Equation 3.2:

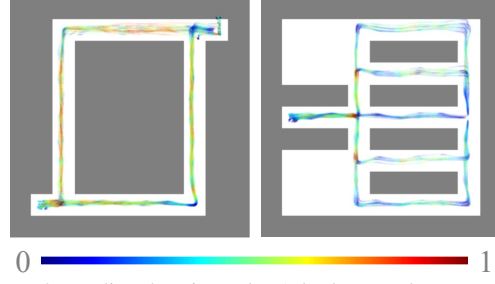


Figure 8. Predicted variance by AdaFlow on the Maze task.

$$\frac{1}{N_t} \frac{1}{N_z} \sum_t \sum_{z_0} \mathbb{E}[\|y - z_0 - v(z_t, t; x)\|^2], \text{ where } z_t = ty + (1 - t)z_0, (x, y) \sim p^*. \quad (17)$$

For each states, we randomly sample 10 time steps ($N_t = 10$) and 10 noises ($N_z = 10$).

A.8. Visualization of Predicted Variance on Maze task.

We present the predicted variance by AdaFlow in Figure 8.

A.9. Additional Experimental Details.

Model Architectures. For the 1D toy example, we used a MLP constructed with 5 fully connected layers and SiLU activation functions. We integrated temporal information by extending the time input into a 100-dimensional time-encoding vector through the cosine transformation of a random vector, $\text{cost} * z_T$, where z_T is sampled from a Gaussian distribution. This time feature is then concatenated with the noise and condition (x) inputs to for time-aware predictions. The network comprises 4 hidden layers, each with 100 neurons, and the output layer predict a single y value. The dataset consists of 10000 single-dimensional samples uniformly distributed in the range $[-5, 5]$.

For navigation and robot manipulation tasks, we adopted the model architecture from Diffusion Policy (Chi et al., 2023). For navigation task, we use the same architecture as used in Push-T task. In the RoboMimic and LIBERO experiments, we used the Diffusion Policy-C architecture. To ensure a fair comparison across different methods, we maintained a consistent architecture for all methods in our experiments, except where specifically noted. Detailed parameters are available in Table 5.

Table 5. Hyperparameters used for training AdaFlow and baseline models.

Hyperparameter	1D Toy			Maze			RoboMimic & LIBERO		
	RF & AdaFlow	BC	Diffusion Policy	RF & AdaFlow	BC	Diffusion Policy	RF & AdaFlow	BC	Diffusion Policy
Learning rate	1e-2	1e-2	1e-2	1e-4	1e-4	1e-4	1e-4	1e-4	1e-4
Optimizer	Adam	Adam	Adam	AdamW	AdamW	AdamW	AdamW	AdamW	AdamW
β_1	0.9	0.9	0.9	0.9	0.9	0.9	0.95	0.95	0.95
β_2	0.999	0.999	0.999	0.999	0.999	0.999	0.999	0.999	0.999
Weight decay	0	0	0	1e-6	1e-6	1e-6	1e-6	1e-6	1e-6
Batch size	1000	1000	1000	256	256	256	64	64	64
Epochs	200	200	400	200	200	200	500(L) / 3000(RM)	500(L) / 3000(RM)	500(L) / 3000(RM)
Learning rate scheduler	cosine	cosine	cosine	cosine	cosine	cosine	cosine	cosine	cosine
EMA decay rate	-	-	-	0.9999	0.9999	0.9999	0.9999	0.9999	0.9999
Number of training time steps	-	-	100	-	-	20	-	-	100
Number of Inference time steps	100 (RF)	-	100(DDPM)	-	-	20(DDPM)	-	-	100(DDPM)
η	0.1	-	-	1.5	-	-	1.0	-	-
ϵ_{\min}	5	-	-	5	-	-	10	-	-
Action prediction horizon	-	-	-	16	16	16	16	16	16
Number of observation input	-	-	-	2	2	2	2	2	2
Action execution horizon	-	-	-	8	8	8	8	8	8
Observation input size	1	1	1	4 (Single-task) / 6(Multi-task)			76 × 76	76 × 76	76 × 76

Implementation of Baselines. In our studies, **BC** was implemented as a baseline, applying behavior cloning in its most straightforward form and using a Mean Squared Error loss function between the predicted and ground truth actions. The implementations for DDPM and DDIM remained consistent with those outlined in Chi et al. (2023). Across all experiments, consistency was maintained regarding architecture, input, and output, with all methods adhering to a similar experimental

pipeline. We just use a 4 layer MLP with SiLU activation for the variance prediction, with hidden dimension of 512, which is a very small network whose computational overhead can be neglected compared to the full model.

Implementation of Variance Prediction Network. In the 1D toy experiment, we designed the variance prediction network as a 4-layer MLP, mirroring the main model’s architecture for simplicity. In theory, the variance estimation network takes the same input as rectified flow model, so its input can be just the intermediate features extracted by the main model. Hence in the navigation and manipulation experiments, the inputs of variance prediction networks are the bottle-neck features extracted by the U-Net model.

Training on RoboMimic. Training Diffusion Models on RoboMimic is very resource-intensive. Training and evaluating a Transport task requires over a month of GPU hours. More complex tasks, such as ToolHang, can demand up to three times longer ¹Given the challenges in replicating the results from (Chi et al., 2023), we opted to start with their open-sourced pretrained model. We then fine-tuned the baselines and our method for 500 epochs and subsequently compared the performance of different models. The full results on all RoboMimic task can be found in Table 6.

Table 6. Full results on the RoboMimic Benchmark. The highest success rate for each task are highlighted in **bold**. For tasks marked with *, we train the model for 500 epochs due to prohibitive training cost.

	NFE↓	Lift ph / mh	Can ph / mh	Square ph / mh	Transport* ph / mh	ToolHang* ph	Push-T ph
LSTM-GMM	1	1.00 / 1.00	1.00 / 1.00	0.95 / 0.86	0.76 / 0.62	0.67	0.69
IBC	1	0.79 / 0.15	0.00 / 0.01	0.00 / 0.00	0.00 / 0.00	0.00	0.75
BET	1	1.00 / 1.00	1.00 / 1.00	0.76 / 0.68	0.38 / 0.21	0.58	-
<i>Same network architecture</i>							
BC	1	1.00 / 1.00	1.00 / 0.96	0.92 / 0.96	0.90 / 0.80	0.78	0.98
Diff- π	100	1.00 / 1.00	1.00 / 1.00	1.00 / 0.97	0.90 / 0.72	0.90	0.91
Diff- π	1	0.04 / 0.04	0.00 / 0.00	0.00 / 0.00	0.00 / 0.00	0.00	0.04
Diff- π	2	0.64 / 0.98	0.52 / 0.66	0.56 / 0.12	0.84 / 0.68	0.68	0.34
AdaFlow	1.17	1.00 / 1.00	1.00 / 0.96	0.98 / 0.96	0.92 / 0.80	0.88	0.96

A.10. Comparison with standard Rectified Flow.

For the purpose of policy learning, we can consider standard Rectified Flow as a subset of our method, which can be recovered with specific choices of η and ϵ_{\min} . In this section, we compare our approach with the standard Rectified Flow, particularly focusing on the generation within a single step. Standard Rectified Flow requires a reflow or distillation stage to straighten the ODE process. During this reflow stage, the model simulates data using the initial 1-Rectified Flow. These data are then used in distillation training, resulting in what is termed a 2-Rectified Flow. Theoretically, a 2-Rectified Flow is capable of producing a straight generation trajectory, which enables one-step generation. In contrast, the 1-Rectified Flow tends to be less straight, necessitating multiple steps for sample generation.

In Table 7, we compare the performance of 1-Rectified Flow, 2-Rectified Flow, and our method in the maze task. Furthermore, Figure 9 illustrates the trajectories produced by both standard Rectified Flow and our method. It’s evident that the standard 1-Rectified Flow struggles to generate a diverse range of actions in a single step. In contrast, our method is able to produce diverse behaviors in nearly one step. This efficiency is attributed to our method’s ability to estimate the variance across different states, identifying those that require multi-step generation.

A.11. Comparison with other 1-step diffusion models.

Recent studies have focused on developing methods for the low-NFE regime. These include the use of ODE-solvers (Press & Teukolsky, 1992), distillation methods (Salimans & Ho), and 1-step diffusion models (Song et al., 2023). ODE-solvers, such as adaptive methods, can reduce NFE during inference, but they theoretically cannot simplify an ODE’s entire solution process to a single step. Distillation-based approaches, similar to Rectified Flow, necessitate the creation of synthetic data for distillation. This process is resource-intensive, as it requires simulating the entire ODE.

Among these methods, Consistency Models have shown potential in single-step generation for image generation without needing distillation. Here, we investigate the application of such a model for decision-making problems. As in our 1D toy

¹See [this link](#)

Table 7. Performance on maze navigation tasks. The table showcases the success rate (**SR**) for each model across different maze complexities. Additionally, for single-task mazes (e.g., Maze 1 and Maze 2), we evaluate the diversity score (**DS**) to reflect the model’s capacity to learn diverse behavior. The highest success rate and diversity score for each task are highlighted in **bold**. Note that 2-RF needs an expensive distillation training stage.

		Maze 1	Maze 2	Maze 3	Maze 4
	NFE↓	SR↑ / DS↑	SR↑ / DS↑	SR↑	SR↑
1-RF	1	1.00 / 0.52	1.00 / 0.49	0.98	0.80
1-RF	5	0.82 / 0.98	1.00 / 0.95	0.94	0.80
2-RF (distill)	1	0.82 / 0.98	1.00 / 0.98	1.00	0.80
AdaFlow ($\eta = 1.5$)	1.56	0.98 / 0.92	1.00 / 0.86	0.96	0.86
AdaFlow ($\eta = 2.5$)	1.12	1.00 / 0.91	1.00 / 0.85	0.94	0.78

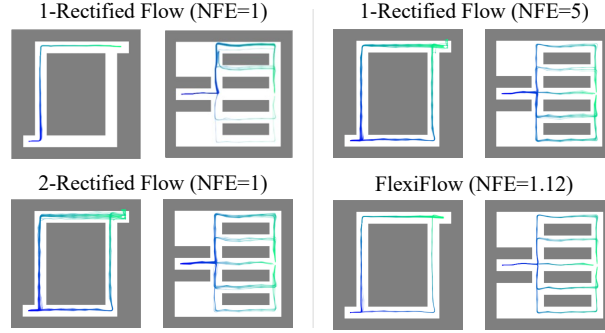


Figure 9. **Generated trajectories.** We visualize the trajectories generated by standard Rectified Flow and AdaFlow, with the agent’s starting point remaining fixed.

experiment, we applied consistency training to it, with the fitting results displayed in Figure 10. To effectively train these models, we made several adjustments to the original settings. These specific parameter modifications are detailed in Table 8. The model appears to struggle with accurately fitting the data, possibly due to its foundation in EDM, a class of models primarily optimized for image generation. While Consistency Models theoretically can facilitate single-step generation, their practical application in decision-making remains challenging due to inherent complexities. AdaFlow offers a more straightforward and easier approach, reducing the need for extensive hyperparameter tuning.

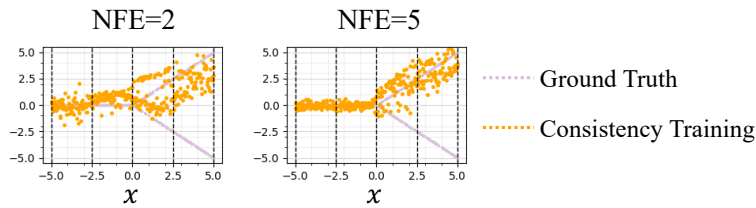


Figure 10. Comparison of ground truth and predicted y values by Consistency Training.

Table 8. Hyperparameters used for Consistency Training.

Hyperparameter	CT
Learning rate	3e-3
Optimizer	AdamW
β_1	0.9
β_2	0.999
Weight decay	0
Batch size	1000
Epochs	1000
EMA decay rate	0.9
Time steps ²	$(\sigma_{\min}^{\frac{1}{\rho}} + \frac{i}{N-1}(\sigma_{\max}^{\frac{1}{\rho}} - \sigma_{\min}^{\frac{1}{\rho}}))^{\rho}$
Skip scaling $c_{\text{skip}}(\sigma)$	$\sigma_{\text{data}}^2 / (\sigma^2 + \sigma_{\text{data}}^2)$
Output scaling $c_{\text{out}}(\sigma)$	$\sigma \cdot \sigma_{\text{data}} / \sqrt{\sigma^2 + \sigma_{\text{data}}^2}$
Input scaling $c_{\text{IN}}(\sigma)$	$1 / \sqrt{\sigma^2 + \sigma_{\text{data}}^2}$
Noise condition	$\frac{1}{4} \ln \sigma$
Schedule functions $N(\cdot)$	$N(k) = \lfloor \sqrt{\frac{k}{K}((s_1 + 1)^2 - s_0^2) + s_0^2 - 1} \rfloor + 1$
Initial discretization steps s_1	150
Target discretization steps s_0	2
Other parameters	$\sigma_{\min} = 0.002, \sigma_{\max} = 80$ $\sigma_{\text{data}} = 0.5, \rho = 7$